arXiv:1403.5870v1 [cond-mat.str-el] 24 Mar 2014

Tunable "rotons" in square lattice antiferromagnets under strong magnetic fields

Yurika Kubo*and Susumu Kurihara
Department of Physics, Waseda University, 3-4-1 Okubo, Shinjuku, Tokyo 169-8555, Japan

March 25, 2014

Abstract

Excitation spectra of square lattice Heisenberg antiferromagnets in magnetic fields are investigated by the spin wave theory. It is pointed out that a rotonlike structure appears in a narrow range of magnetic fields, as a result of strong nonlinear effects. It is shown that the energy gap and the mass of the "roton" are quite sensitive to the magnetic field: the roton gap softens rapidly and eventually closes as a precursor of a quantum phase transition. The possibility of the experimental observation of the roton and a new ground state after its softening are discussed.

1 INTRODUCTION

Square lattice Heisenberg antiferromagnets (SLHAFs) are well known to have the Néel order at zero field, and their excitation spectra are well described by the linear spin wave (LSW) theory with small renormalization [1]. However, an external magnetic field induces noncollinear structure resulting in nonlinear three-magnon interactions [2, 3]. It should be stressed that the three-magnon interactions in SLHAFs can be controlled, from zero to sufficiently large values, simply by tuning external magnetic fields [2–5]. These features are in sharp contrast with the triangular lattice antiferromagnets, which have a noncollinear 120 degree structure, and therefore have strong nonlinear interactions even for zero field [6,7]. Accordingly, SLHAF is an ideal system to examine the effects of the three-magnon interactions.

Theoretical calculations [2, 3, 5, 8] and experiments [9, 10] on excitation spectra of SLHAF in fields show significant deviations from that of the LSW calculations. Frustration-induced noncollinear antiferromagnets also show such deviations [6, 7, 11, 12].

Zhitmirsky *et al* [3] and Mourigal *et al* [2] proposed several methods to calculate the magnon spectra in high fields, where the three-magnon interactions are strong [2–4, 13]. However, a self-consistent Born approximation (SCBA), which neglects vertex corrections, results in an unphysical gap in the acoustic mode [3]. This is due to a violation of the Ward-Takahashi identity, suggesting crucial importance of vertex corrections in such renormalization. Mourigal *et al* [2] partially perform SCBA for $S \geq 1$, still neglecting vertex corrections, and consider only the imaginary part of self-energy. They thus remove the unphysical gap [2], but do not essentially solve the problem of the violation of the Ward-Takahashi identity. Lastly, Fuhrman *et al* [13] introduce an alternative idea of adding some interlayer interactions, rendering the system essentially three-dimensional. This, however, can not be the solutions to the difficulty in purely two-dimensional model, and we still lack reliable results.

We believe that the perturbation calculation is much more reliable than that of partial renormalization of self-energy, since the former satisfies the Ward-Takahashi identity albeit in a trivial way. Thus, we calculate the nonlinear spin wave spectra of the purely two-dimensional SLHAFs in fields within the simple second order perturbation theory on the basis of the Zhitmirsky-Mourigal formalism [2, 3].

Our calculation shows that a rotonlike minimum emerges in a quite narrow range of fields at about 3/4 of the saturation field H_s, a remarkable feature in the magnon spectrum which previous works [2,3,5,8] might have overlooked. We also find that the roton gap drops steeply to zero as the field increases.

This paper is composed as follows. First, we briefly introduce the spin wave formalism following Zhitomirsky and Mourigal *et al*. Then, we show how the spin wave spectra vary with fields within the second order perturbation calculation. The main feature of the spectra is an appearance of a rotonlike minimum which responds sensitively to small changes of fields. Lastly, we discuss a new ground state after the softening of the roton and possibilities to detect it by experiments.

2 MODEL

In this section, main points of Zhitmirsky-Mourigal formalism on SLHAFs [2, 3] are summarized. Heisenberg Hamiltonian in a magnetic field H is:

$$\hat{\mathcal{H}} = J \sum_{<i,j>} \mathbf{S}_i \cdot \mathbf{S}_j - H \sum_i S_i^{z_0}, \qquad (1)$$

where $S_i^{\mu}(\mu = x_0, y_0, z_0)$ denote spin operators in the laboratory frame and J denotes the nearest neighbor exchange constant. Then, we move from the laboratory frame to the rotating frame with spin operators

*E-mail: kubo@kh.phys.waseda.ac.jp

S_i^{μ} ($\mu = x, y, z$):

$$\begin{aligned} S_i^{x_0} &= S_i^x \sin\theta + S_i^z e^{i\mathbf{Q}\cdot\mathbf{R}_i}\cos\theta, \qquad S_i^{y_0} = S_i^y, \\ S_i^{z_0} &= -S_i^x e^{i\mathbf{Q}\cdot\mathbf{R}_i}\cos\theta + S_i^z \sin\theta, \end{aligned} \tag{2}$$

where $\mathbf{Q} = (\pi, \pi)$ denotes the ordering wave vector. The canting angle θ is chosen to minimize the ground state energy:

$$\theta = \sin^{-1}[h], \qquad h = H/H_s, \qquad H_s = 8JS. \tag{3}$$

We then perform the Holstein-Primakoff (HP) transformation:

$$\begin{aligned} S_i^+ &= \sqrt{2S - a_i^\dagger a_i}\, a_i, \qquad S_i^z = S - a_i^\dagger a_i, \\ S_i^- &= a^\dagger \sqrt{2S - a_i^\dagger a_i}, \end{aligned} \tag{4}$$

where a_i denotes HP bosons. We get

$$\hat{\mathcal{H}} = \sum_{n=0}^{\infty} \hat{\mathcal{H}}_n, \tag{5}$$

where $\hat{\mathcal{H}}_n$ denotes the n-th order term in HP boson operators [2], and $\hat{\mathcal{H}}_1$ vanishes by determining θ correctly [2, 3, 14].

We perform the Fourier transformation and then, the Bogoliubov transformation [2, 3, 14]:

$$a_{\mathbf{k}} = u_{\mathbf{k}} b_{\mathbf{k}} + v_{\mathbf{k}} b_{-\mathbf{k}}^\dagger, \qquad \left(u_{\mathbf{k}}^2 - v_{\mathbf{k}}^2 = 1\right), \tag{6}$$

where $b_{\mathbf{k}}$ denotes Bogoliubov bosons. $\hat{\mathcal{H}}_2$ is readily diagonalized yielding an excitation spectrum:

$$\begin{aligned} &\epsilon_{\mathbf{k}} = \sqrt{A_{\mathbf{k}}^2 - B_{\mathbf{k}}^2}, \qquad \gamma_{\mathbf{k}} = \frac{\cos k_x + \cos k_y}{2}, \\ &A_{\mathbf{k}} = 4JS(1 + \gamma_{\mathbf{k}} \sin^2\theta), \;\; B_{\mathbf{k}} = 4JS\,\gamma_{\mathbf{k}} \cos^2\theta. \end{aligned} \tag{7}$$

We now focus on the three-magnon interaction Hamiltonian $\hat{\mathcal{H}}_3$:

$$\begin{aligned} \hat{\mathcal{H}}_3 =& \frac{1}{2!}\sum_{\mathbf{k},\mathbf{p}} (b_{\mathbf{q}}^\dagger b_{\mathbf{p}_1}^\dagger b_{\mathbf{k}} + \text{H.c.}) \Phi_1(\mathbf{k}, \mathbf{p_1}, \mathbf{q}) \\ &+ \frac{1}{3!}\sum_{\mathbf{k},\mathbf{p}} (b_{\mathbf{k}}^\dagger b_{\mathbf{p}_2}^\dagger b_{\mathbf{q}}^\dagger + \text{H.c.}) \Phi_2(\mathbf{k}, \mathbf{p_2}, \mathbf{q}), \end{aligned} \tag{8}$$

where $\mathbf{p}_1 = \mathbf{Q} + \mathbf{k} - \mathbf{q}$, $\mathbf{p}_2 = \mathbf{Q} - \mathbf{k} - \mathbf{q}$ and $\Phi_\alpha(1, 2, 3) \propto \sin 2\theta$ ($\alpha = 1, 2$) are given in Refs. 2 and 3, and they come into play only with noncollinear magnetic structures. Self-energy corrections, which is generated by Eq. (8), are [2, 3]:

$$\Sigma^{(1)}(\mathbf{k}, \omega) = \frac{1}{2}\sum_{\mathbf{k}} \frac{|\Phi_1(\mathbf{k}, \mathbf{p}_1, \mathbf{q})|^2}{\omega - \epsilon_{\mathbf{p}_1} - \epsilon_{\mathbf{q}} + i0}, \tag{9}$$

$$\Sigma^{(2)}(\mathbf{k}, \omega) = -\frac{1}{2}\sum_{\mathbf{k}} \frac{|\Phi_2(\mathbf{k}, \mathbf{p}_2, \mathbf{q})|^2}{\omega + \epsilon_{\mathbf{p}_2} + \epsilon_{\mathbf{q}} - i0}. \tag{10}$$

Lowest order $1/S$ corrections generated by three-magnon couplings are given by following on shell self-energy:

$$\Sigma_{\mathbf{k}} = \Sigma^{(1)}(\mathbf{k}, \epsilon_{\mathbf{k}}) + \Sigma^{(2)}(\mathbf{k}, \epsilon_{\mathbf{k}}). \tag{11}$$

We see from Eqs. (9) and (11) that its corrections are especially strong with a smaller energy difference between an initial and intermediate state.

We also need to perform the Hartree-Fock decoupling in $\hat{\mathcal{H}}_4$ leading to a correction $\delta\epsilon_{\mathbf{k}}^{\text{HF}}$, and take quantum corrections to the canting angle into account, yielding another correction $\delta\epsilon_{\mathbf{k}}^{\theta}$. Finally, we get the $1/S$ corrected spin wave spectra [2, 3, 14]

$$\bar{\epsilon}_{\mathbf{k}} = \epsilon_{\mathbf{k}} + \Sigma_{\mathbf{k}} + \delta\epsilon_{\mathbf{k}}^{\text{HF}} + \delta\epsilon_{\mathbf{k}}^{\theta}. \tag{12}$$

3 MIXING OF THE ONE- AND TWO-MAGNON STATE

The effects of the coupling between one-and two-magnon states on $\bar{\epsilon}_{\mathbf{k}}$ become quite strong at around $h \approx 0.75$. There are two reasons for this. First, $\Phi_1(1, 2, 3) \propto \sin 2\theta$ [2, 3], which reflects the strength of hybridizations, takes the maximum value at around $h \approx 0.75$. Second, the curvature on the acoustic mode become positive also for $h \gtrapprox 0.75$ [2–4]. The relation between the positive curvature and the strong couplings is briefly discussed below based on the previous works [2–4].

The curvature on the acoustic mode, which is highest along the Γ-M = (π, π) line, increases monotonically as the field increases. Simultaneously, the effects of the nonlinear interactions also increase, since the higher curvature induces the stronger three-magnon interactions. The curvature changes its sign from negative to positive, which first occurs at $h^* = 2/\sqrt{7} \approx 0.7559$ along the Γ-M line. The positive curvature cause a spontaneous magnon decay which satisfies the kinematic constraint:

$$\epsilon_{\mathbf{k}} = \epsilon_{\mathbf{q}} + \epsilon_{\mathbf{Q}-\mathbf{q}+\mathbf{k}}. \tag{13}$$

We note that an especially strong mixing of the one- and two-magnon states are expected near the threshold of the decay region, where the energy conservation law holds, since there are many processes which have infinitesimal energy differences between the initial and intermediate states [see Eq. (9)]. Consequently, we focus on an intersection point of the decay threshold with the Γ-M line, where the particularly strong hybridizations between the states are expected.

4 APPEARANCE AND SOFTENING OF "ROTONS" IN STRONG MAGNETIC FIELD

Now, we discuss the magnon spectrum $\bar{\epsilon}_{\mathbf{k}}$ renormalized by three-magnon couplings given in Eq. (11), corresponding to the $1/S$ corrections coming from the Holstein-Primakoff expansion of spin operators.

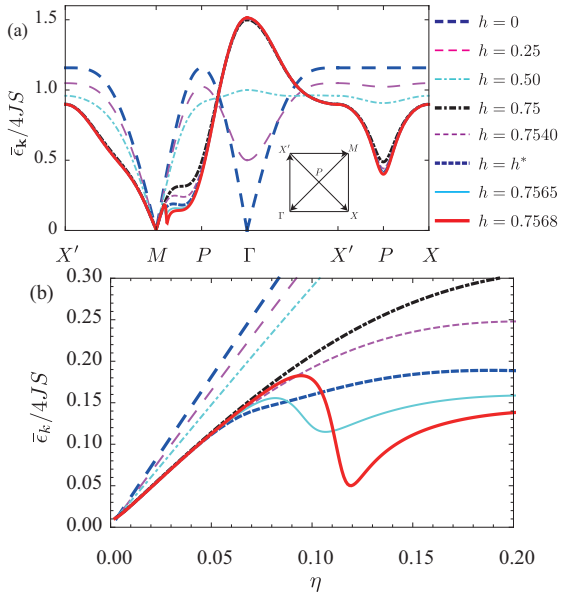

Figure 1: (Color online) (a) Nonlinear spin wave spectra $\bar{\epsilon}_{\mathbf{k}}$ for the $S = 1/2$ system along the highly symmetric line calculated for several magnetic fields. The magnetic field h corresponding to each line is shown on the right side. The spectrum along the Γ-M line near the M point varies drastically during small changes of h. There are apparent minima at the P point along the X-X' line at finite fields. (b) Enlarged $\bar{\epsilon}_{\mathbf{k}}$ for $S = 1/2$ SLHAF along the Γ-M line near the M point [$\pi(1-\eta, 1-\eta)$ $0 \le \eta \le 0.20$].

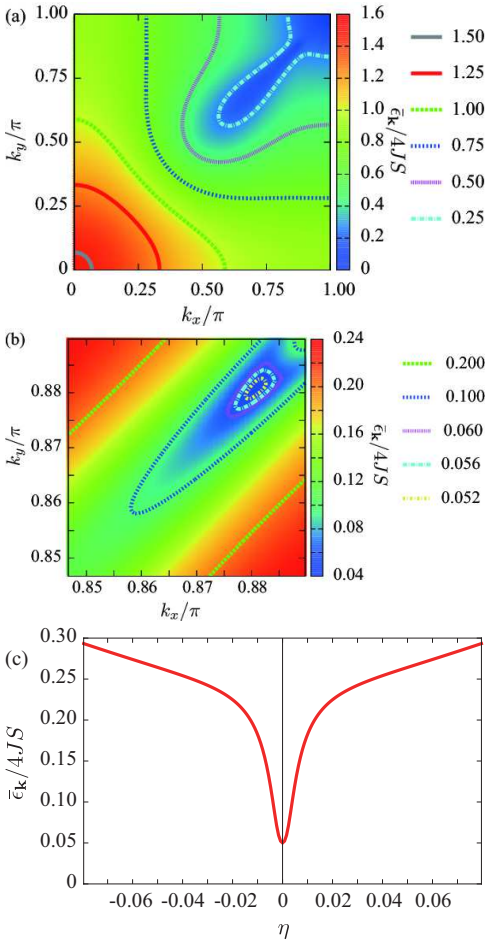

Figure 2: (Color) (a) Contour plot of $\bar{\epsilon}_{\mathbf{k}}$ ($S = 1/2$, $h = 0.7568$) of the whole Brillouin zone. The energy corresponding to each contour is shown on the right side. (b) Enlarged contour plot of $\bar{\epsilon}_{\mathbf{k}}$ ($S = 1/2$, $h = 0.7568$) near the M point. It is now clear that an energy minimum appears near the M point. (c) Enlarged $\bar{\epsilon}_{\mathbf{k}}$ ($S = 1/2$, $h = 0.7568$) along the line $\pi(\eta_{\rm rot}-\eta, \eta_{\rm rot}+\eta)$, where $\eta_{\rm rot}$ denotes a roton wave vector $\pi\eta_{\rm rot}(1,1)$, perpendicular to the Γ-M line. Note the sharpness of the minimum along this direction; half width is on the order of 0.01.

4.1 Appearance of a rotonlike minimum

Fig. 1(a) shows the spectra for the $S = 1/2$ SLHAF, calculated for several magnetic fields h. Rotonlike structure emerges near the M point, which is enlarged in Fig. 1(b) for clarity. Very sensitive responses to slight changes of h are seen along the Γ-M line while little change along the others. Therefore, we focus on $\bar{\epsilon}_{\mathbf{k}}$ along the Γ-M line. Enlarged spectra $\bar{\epsilon}_{\mathbf{k}}$ in Fig. 1(b) remind us of the roton in the superfluid Helium [15]. We find that the wave vector, gap and mass of a rotonlike structure changes drastically during less than 1% change of the magnetic field h near $h^* = 2/\sqrt{7}$. The gap gets smaller and smaller by increasing fields and finally vanishes, which indicates a quantum phase transition characterized by a certain modulation of the ground state.

Contour plot of $\bar{\epsilon}_{\mathbf{k}}$ ($S = 1/2, h = 0.7568$) of the whole Brillouin zone is shown in Fig. 2(a). We see that the strong three-magnon couplings at around $h \approx 0.75$ induce anisotropic spectra along the Γ-M line. We also show an enlarged $\bar{\epsilon}_{\mathbf{k}}$ near the M point in Fig. 2(b). It is now clear that the minimum near the M point is in fact a local minimum in two-dimensional Brillouin zone, thus deserving the name roton. Fig. 2(c) shows the roton spectrum near the roton wave vector along the line perpendicular to the Γ-M line. We note that the minimum is much sharper along this line, with half width of order 0.01. We discuss the origin of the sharpness in the next subsection. We also observe apparent minima at the point P [$(\pi/2, \pi/2)$] along the X-X' line. However, the P point is not really a local minimum in the Brillouin zone, since it is on a downhill slope along the Γ-M line.

Rotonlike minima near the M point have not been reported, to our knowledge. This might be due to the extreme narrowness of the field range where the roton can exist. Concerning the P point features, recently synthesized, almost ideal SLHAF $Cu(pz)_2(ClO_4)_2$ exhibits stronger response to fields on the P point than that of the X' point [10]. This is qualitatively consistent to our results of Fig. 1(a) and Refs. 2 and 5.

Dependence of the magnon spectra on spin magnitude S is shown for $S = 1/2$ to $S = \infty$ (LSW result) for $h = 0.7568$ in Fig. 3. Stronger $1/S$ corrections are observed along the Γ-M line than the others and more clas-

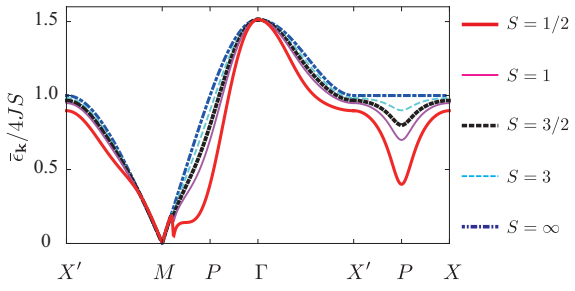

Figure 3: (Color online) (a) Nonlinear spin wave spectra $\bar{\epsilon}_{\mathbf{k}}$ for the various S including $S = \infty$ (LSW) at $h = 0.7568$. Spin magnitude S for each line is shown on the right side. Spectra become more classical for larger S, but no qualitative changes are observed. It is also suggested that the quantum effects are stronger along the Γ-M line than the others.

sical results are obtained for larger S. However, qualitatively the same behaviors are observed for various S.

4.2 Details of the roton spectrum

We examine how the roton, which appears only in the range of less than 1% of the saturation field, varies sensitively with field h. Here, rotons emerge also for $S > 1$, but we focus on $S = 1/2$ and $S = 1$ rotons for a while. Roton gap $\Delta_{\rm rot}$ and wave vector $\tilde{\mathbf{k}}_{\rm rot}$ as functions of h are shown in Figs. 4(a) and (b). We denote $\mathbf{q}/\tilde{\mathbf{q}} = \mathbf{Q} - \mathbf{q}$ as a wave vector measured from the M/Γ point from this subsection. Roton mass perpendicular/parallel to the Γ-M line $m^*_\perp/m^*_\parallel$ as functions of h are shown in Fig. 4(c) and (d), where solid points represent $m^*_\perp$ and open points represent $m^*_\parallel$.

We notice that $\Delta_{\rm rot}$ drops steeply to zero, reflecting the increasing three-magnon interactions. We also notice that $\tilde{\mathbf{k}}_{\rm rot}$ appears approximately at the wave vector of the decay threshold $\tilde{\mathbf{k}}_{\rm th}$, where the three-magnon interactions are especially strong because of the infinitesimal energy differences of the initial and intermediate states. $m^*_\perp$ and $m^*_\parallel$ for both $S = 1/2$ and $S = 1$ also drop steeply and $m^*_\parallel$ decrease more rapidly than $m^*_\perp$. It is also notable that roton masses are quite small which means that an extremely sharp structure appears near $\tilde{\mathbf{k}}_{\rm rot}$

In the case of quantum limit, $S = 1/2$, another roton (shallow roton) emerges and its $\tilde{\mathbf{k}}_{\rm rot}$ and $m^*_\parallel$ changes non-monotonically while $\Delta_{\rm rot}$ and $m^*_\perp$ decreases monotonically as h increases. The former behavior is due to the competition between a smaller energy difference between the two states on the side of the M point and a stronger spectral weight on the side of the Γ point, and the latter is due to the increasing nonlinear interactions with increasing h. In addition, the shallow roton also emerges at around $h \approx 0.5$ near the Γ points along the Γ-M line. However, the shallow rotons may easily disappear with finite interlayer couplings or finite temperature effects. Thus, we do not discuss them hereafter, and focus on the ordinary rotons.

First, we examine $\tilde{\mathbf{k}}_{\rm rot}$ by using the fact that $\tilde{\mathbf{k}}_{\rm rot} \approx \tilde{\mathbf{k}}_{\rm th}$. The expanded LSW spectrum $\epsilon_{\tilde{\mathbf{k}}}$ at around the M point [2, 4] up to fifth order in k along the Γ-M line is given by:

$$\epsilon_{\tilde{\mathbf{k}}} \approx ck(1 + \alpha k^2 + \beta k^4),$$

where

$$\begin{aligned} c &= 2JS\sqrt{2}\cos\theta, \\ \alpha &= \frac{1}{12\cos\theta}\left[\left(\frac{h}{h^*}\right)^2 - 1\right], \\ \beta &= \frac{h^4 - 32h^2 + 16}{7680\cos^2\theta}. \end{aligned} \tag{14}$$

The threshold wave vector $\tilde{\mathbf{k}}_{\rm th}$ is determined by [2]:

$$\epsilon_{\tilde{\mathbf{k}}} - 2\epsilon_{\tilde{\mathbf{k}}/2} = 0. \tag{15}$$

Then, we approximate Eq. (15) by using Eq. (14):

$$\epsilon_{\tilde{\mathbf{k}}} - 2\epsilon_{\tilde{\mathbf{k}}/2} \approx \frac{3}{4}k^3 c\left(\alpha + \frac{5}{4}\beta k^2\right). \tag{16}$$

We define an approximate value $\tilde{\mathbf{k}}_0$ of the threshold wave vector $\tilde{\mathbf{k}}_{\rm th}$ by taking the left-hand side of Eq. (16) zero:

$$k_0 = \sqrt{\frac{-4\alpha}{5\beta}} \propto \left[\left(\frac{h}{h^*}\right)^2 - 1\right]^{1/2} \quad (h^* \le h \le 1). \tag{17}$$

This approximation is valid for sufficiently small k_0. The wave vectors $k_{\rm th}$ and k_0 merge asymptotically for $h \to h^*$ in Fig. 4(b).

We now clarify the field dependence of $\Delta_{\rm rot}$, where a derivation is given in Appendix A. We focus on lowest order self-energy corrections shown in Fig. 5:

$$\delta\epsilon_{\tilde{\mathbf{k}}_0} = \Sigma^{(1)}(\tilde{\mathbf{k}}_0, \epsilon_{\tilde{\mathbf{k}}_0}). \tag{18}$$

in the limit of $\mathbf{q} \to 0$, whose corrections are expected to be strong near $\tilde{\mathbf{k}}_{\rm rot}$.

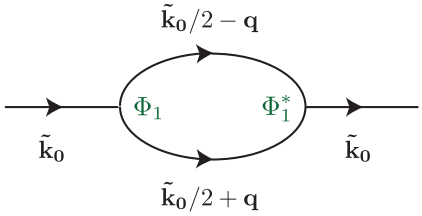

Figure 5: (Color online) Self-energy causing strong renormalization near the roton wave vector.

We perform the approximations:

$$\sqrt{\frac{A_{\tilde{\mathbf{k}}} + B_{\tilde{\mathbf{k}}}}{A_{\tilde{\mathbf{k}}} - B_{\tilde{\mathbf{k}}}}} = \sqrt{\frac{1 - \gamma_{\mathbf{k}}}{1 + \cos 2\theta\gamma_{\mathbf{k}}}} \approx \frac{k}{2\sqrt{2}\cos\theta}, \tag{19}$$
$$\gamma_{\tilde{\mathbf{k}}} \approx -1,$$

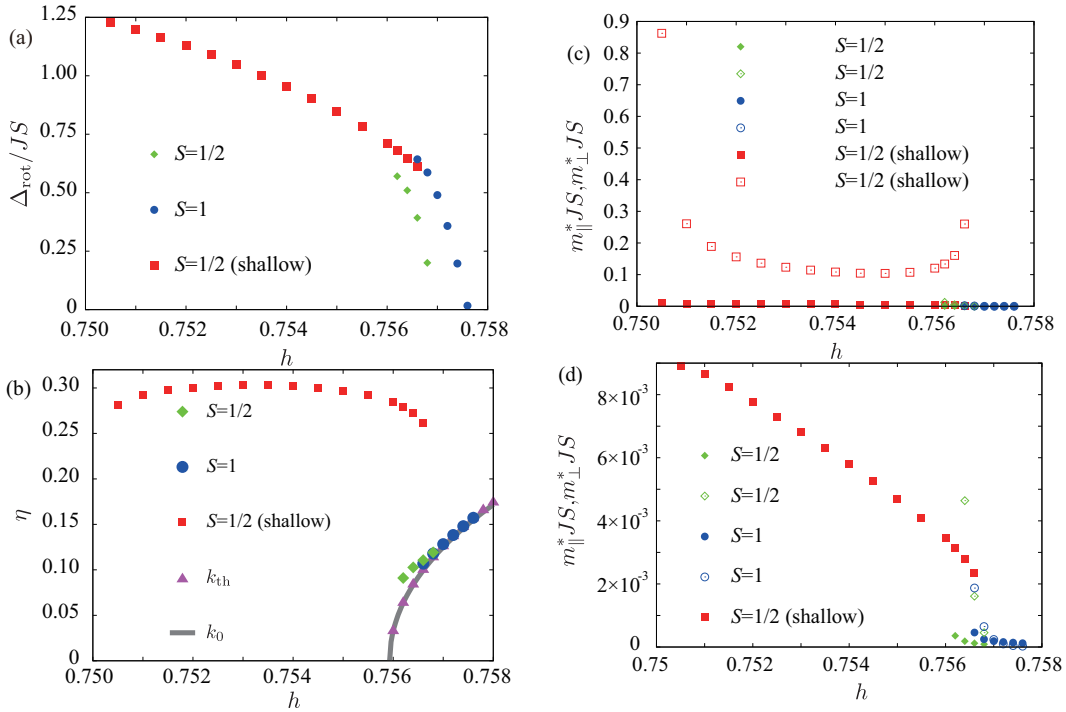

Figure 4: (Color online) (a) Roton gap $\Delta_{\rm rot}$ along the Γ-M line as a function of the field h. Solid diamonds, circles and squares represent results for $S = 1/2$, $S = 1$ rotons, and shallow rotons which appears only for $S = 1/2$. Each roton gap decreases monotonically as the field increases. (b) Roton wave vector along the Γ-M line $[\pi(1-\eta, 1-\eta) \;\; 0 \le \eta \le 1]$ as a function of h. Solid triangular points and a gray line correspond to $k_{\rm rot}$ and k_0. We notice that $k_{\rm rot}$ appears in the neighborhood of $k_{\rm th}$. Little change in $k_{\rm rot}$ is observed for the shallow roton. (c) Roton masses as functions of h, where solid/open points correspond to $m^*_{\perp}/m^*_{\parallel}$. The masses are quite small and non-monotonic behavior is observed for the shallow roton. (d) Roton masses $m^*_{\parallel}$, $m^*_{\perp}$ as functions of h.

to the matrix elements of Eq. (18). We denote

$$\Phi_1\left(\tilde{\mathbf{k}}_0, \mathbf{q}\right) = \Phi_1\left(\tilde{\mathbf{k}}_0, \tilde{\mathbf{k}}_0/2+\mathbf{q}, \tilde{\mathbf{k}}_0/2-\mathbf{q}\right). \tag{20}$$

for simplicity. We get:

$$\frac{\left|\Phi_1\left(\tilde{\mathbf{k}}_0, \mathbf{q}\right)\right|^2\Big|_{\mathbf{q}\to 0}}{J^2 S\,(\sin 2\theta)^2} \approx \frac{k_0^3}{(2\sqrt{2}\cos\theta)^3}. \tag{21}$$

We then approximate the denominator of $\delta\epsilon_{\tilde{\mathbf{k}}_0}$ [2]:

$$\begin{aligned} w[\tilde{\mathbf{k}}_0, \mathbf{q}] &= \epsilon_{\tilde{\mathbf{k}}_0} - \epsilon_{\tilde{\mathbf{k}}_0/2+\mathbf{q}} - \epsilon_{\tilde{\mathbf{k}}_0/2-\mathbf{q}} \\ &\approx -\frac{2c}{k_0}\frac{q^2}{1-(2q/k_0)^2}[\phi^2 - \phi_0^2], \end{aligned}$$

where ϕ denotes an azimuthal angle and

$$\phi_0 = \sqrt{6\alpha}\frac{(k_0/2)^2 - q^2}{q}. \tag{22}$$

We obtain lowest order self-energy corrections:

$$\begin{aligned} \delta\epsilon_{\tilde{\mathbf{k}}_0} &\propto -Jk_0^4\tan^2\theta\int\frac{q\mathrm{d}q}{q^2} \\ &= Jk_0^4\tan^2\theta\ln\left[\frac{\Lambda}{k_0}\right], \end{aligned} \tag{23}$$

where Λ denotes a lower cutoff. We see that the roton is related to a logarithmic factor, which originates from a two-dimensionality [2–4, 13].

Now, we get an approximation to $\Delta_{\rm rot}$:

$$\Delta_{\rm rot} \approx ck_0 + A_0 \cdot Jk_0^4\tan^2\theta\ln\left[\frac{\Lambda}{k_0}\right], \tag{24}$$

where A_0 denotes a constant. Fig. 6(a) shows that $\Delta_{\rm rot}$ decreases proportionally to k_0^4. It is clear that the factor k_0^4 drives the softening. We also see that the logarithmic factor behaves almost as a constant in the region shown in Fig. 6(a), and does not have any singularity there.

The perturbation calculation still works well with a sufficiently small k_0. However, k_0 increases as h/h^* increases [see Eq. (17)], and finally the perturbation calculation on the basis of the simple canted state becomes no longer valid (even for $S > 1$) indicating a new ground state, which might be characterized by modulations with the roton wave vector $\mathbf{k}_{\rm rot}$. We thus see that the roton is essential in determining the new ground state at higher fields. In adddition, $S = 1/2$ roton gap decreases about two times faster than $S = 1$ roton gap, since the dependence on fields is attributed to $1/S$ corrections.

We calculate the perpendicular effective mass $m^*_{\perp}$ by differentiating $\delta\epsilon_{\mathbf{k}}$:

$$m^*_{\perp} \propto k_0^{-2}. \tag{25}$$

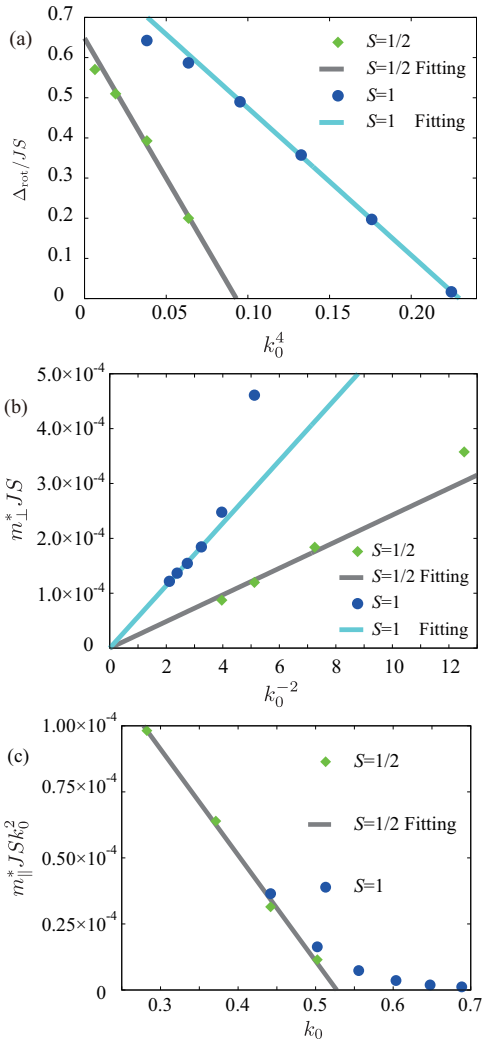

Figure 6: (Color online) (a) Roton gap $\Delta_{\rm rot}$ as a function of k_0^4. Solid diamonds and circles represent $S = 1/2$ and $S = 1$, and lines show fittings using Eq. (24). $S = 1/2$ roton gap decreases about two times faster than $S = 1$ roton gap. (b) Perpendicular mass $m_\perp^*$ as a function of k_0^{-2}; it scales linearly with k_0^{-2}. (c) Parallel mass $m_\parallel^*$ is plotted as $m_\parallel^* k_0^2$ versus k_0. We see that Eq. (26) gives a good approximation to $m_\parallel^*$ for sufficiently small k_0.

Derivation is given in Appendix B. Perpendicular mass $m_\perp^*$ is shown in Fig. 6(b). It is clear that $m_\perp^*$ decreases monotonically with increasing k_0 and its behavior is well described by Eq. (25).

We also calculate the parallel mass $m_\parallel^*$:

$$m_\parallel^* \propto \left[k_0^2(1+b_0k_0)\right]^{-1} \approx k_0^{-2}(1-b_0k_0), \qquad (26)$$

where b_0 denotes a constant. This approximation is valid for sufficiently small k_0. The quantity $m_\parallel^* k_0^2$ is shown as a function of k_0 in Fig. 6(c); it scales linearly with k_0 for sufficiently small k_0.

We have calculated $\Delta_{\rm rot}$, $m_\perp^*$, and $m_\parallel^*$, and our approximations describe their field dependences rather well. In other words, the perturbation calculation and analytical approximation agree reasonably well.

We also discuss the valley-like structure perpendicular to the Γ-M line in Fig. 2(c). Here, we examine $\delta\epsilon_{\tilde{\mathbf{k}}_0}$ given in Eq. (18). We approximate the energy denominator $w[\tilde{\mathbf{k}}_0, \mathbf{q}]$ by using Eq. (22):

$$w[\tilde{\mathbf{k}}_0, \mathbf{q}] \approx -\frac{cqk_0^2}{2}\frac{\phi^2-\phi_0^2}{\phi_0}. \qquad (27)$$

We evaluate the angular integration as:

$$\int \frac{d\phi}{w[\tilde{\mathbf{k}}_0,\mathbf{q}]} \approx -\frac{1}{cqk_0^2}\int d\phi\left(\frac{1}{\phi-\phi_0}-\frac{1}{\phi+\phi_0}\right) \propto \ln\left[|\phi-\phi_0|+\delta\phi\right], \qquad (28)$$

where $\delta\phi$ denotes a cutoff coming from the small difference between $k_{\rm rot}$ and $k_{\rm th}$:

$$\delta\phi \propto k_{\rm rot}/k_{\rm th} - 1. \qquad (29)$$

5 DISCUSSION

We have studied the excitation spectra of SLHAF in fields and have found the appearance and softening of roton as a function of h/h^*. We consider that the roton emerges and softens as a precursor of the phase transition. Then, it seems interesting to determine the new ground state. In this section, the new ground state and possibilities to detect the roton are discussed.

5.1 New ground state

In the classical limit $S = \infty$, the simple canted state is selected to minimize the exchange energy and the Zeeman energy. However, for finite S, the three-magnon interactions are induced by the noncollinear structures. Its effects are strong at around $h \approx 0.75$ especially for the certain wave vector $\tilde{\mathbf{k}}_{\rm rot} \approx \tilde{\mathbf{k}}_0$ causing the roton's appearance.

Previous works on $S = 1/2$ SLHAFs calculate some static properties like the spin stiffness, magnetization, spin wave velocity and so on as functions of fields by exact diagonalization [5] and spin wave calculation [14, 16] and no anomalies are observed at around $h \approx 0.75$. However, a qualitative change between high and low fields is observed in the dynamical structure factor studied by quantum Monte Carlo simulation [8] and exact diagonalization [5].

Considering these results, we expect that the new ground state might be rather similar to the simple canted states and $\mathbf{k}_{\rm rot}$, where the transition occurs, may signify the new ground state. We speculate that a certain modulation with wave vector $\mathbf{k}_{\rm rot}$ occurs in the spin ordering in $S_i^{x_0}$-$S_i^{y_0}$ plane while the canting angle θ remains essentially unchanged. In other words, the new ground state might be characterized by a freezing out of the roton mode. In addition, the new ground state might be similar to the spin-current order discussed in Ref. 17. We believe that roton's appearance and its softening are essentially correct, though they are not quantitatively accurate since these are the results of the second order perturbation calculations.

5.2 Possibilities to detect rotons

Now, we discuss the possibilities to detect rotons by experiments. In the same way as rotons in Helium [15,18], it is possible to detect the rotonlike minimum by inelastic neutron scattering along the Γ-M line and specific heat measurements on the certain conditions. We need proper materials and high accuracy measurements to be discussed below.

We need materials which have a low enough $H_{\rm s}$ to achieve $h \approx 0.75$. Here, the field range, where the roton emerges, is about 0.1% of $H_{\rm s}$ in the field range. Accordingly, we also need the uniformity and control of magnetic field with a precision of order $h \approx 0.001$ at around $h \approx 0.75$.

We also need a very high accuracy in wave vector to detect rotons. This is because of the very sharp structure of the roton spectrum, especially along the direction perpendicular to the Γ-M line. If the resolution in wave vector is worse than the sharpness of the roton, excitation spectrum may acquire an apparent width because of the steepness of the roton spectrum. It should be noted that such width is essentially independent of the magnon decay [2–4]. This may give, at least, a partial explanation of the anomalously large width reported in exact diagonalization study [5] or quantum Monte Carlo simulation [8]

We also note it is also possible to detect rotons for $S > 1$, which appear in higher fields, but the roton masses become smaller with larger k_0 [see Eq. (25)] and therefore we need a more accuracy in wave vectors to detect them. Consequently, we see $S = 1/2$, 1 HAF is the best candidate.

Recently, almost ideal $S = 1/2$ two-dimensional SL-HAFs are synthesized [10, 19]. They might be experimental candidates to examine the properties at high fields, since these compounds have small magnetic anisotropies, interlayer couplings and low enough saturation fields.

We see that it is worth trying to detect the roton, which vary remarkably by slight changes of h, though there may be difficulties. Furthermore, the experiments may find what the new ground state looks like. In addition, it is also stimulating to detect the apparent minima at the point P, which requires a less uniformity and control of the field h, and an accuracy in wave vectors.

6 CONCLUSION

We have investigated the field dependence of the nonlinear spin wave spectrum within the second order perturbation calculation. We have found the rotonlike minimum in the renormalized spectrum at the roton wave vector $k_{\rm rot} \approx k_0$, where three-magnon couplings are particularly strong. We have also calculated $\Delta_{\rm rot}$ and $m_\perp^*$, and found that they change as functions of k_0 (or h/h^*).

We see that the especially strong three-magnon coupling near the point, where the decay threshold meets the Γ-M line, causes the appearance of rotons accompanied by the logarithmic factor. Furthermore, the coupling increases as the field increases triggering the softening of the roton. Thus, we consider that the roton is physically quite important. Though deciding the modulated ground state is beyond the scope of this paper, we expect that $\mathbf{k}_{\rm rot}$, when the modulation occurs, signifies what is the new ground state like.

We have also found the valley-like structure perpendicular to the Γ-M line near the $\mathbf{k}_{\rm rot}$. We see that the sharp structure near the $\mathbf{k}_{\rm rot}$ may induce the apparent linewidth of experiments and numerical results [5, 8, 9]. We expect that the anomalously large linewidth reported in the previous works [5, 8, 9] might be partially explained by its sharp structure even in the absence of magnon decay.

The emergence and the softening the roton feature in the spin wave spectrum is quite important at low temperatures and high fields. By carefully tuning the magnetic field, it will be possible to see the roton effects in low temperature specific heats, neutron scattering, and spin transport [20]. Among other things we expect that the rotons may be most easily detected as an exponential temperature dependence in thermal and transport properties.

A ESTIMATION OF ROTON GAP

We derive how $\Delta_{\rm rot}$ depends on k_0. We perform the approximation given in Eq. (19) to the matrix elements of $\delta\epsilon_{\tilde{\mathbf{k}}_0}$ obtaining

$$\frac{2NS\left|\Phi_1(\tilde{\mathbf{k}},\tilde{\mathbf{q}},\tilde{\mathbf{p}})\right|^2}{(H\cos\theta)^2} \approx \frac{9\,\tilde{k}\tilde{q}\tilde{p}}{4\,(2\sqrt{2}\cos\theta)^3}, \tag{30}$$

where N denotes the number of sites and $\tilde{\mathbf{p}} = \tilde{\mathbf{k}} - \tilde{\mathbf{q}}$.

Then, we consider the process in Fig. 5. We write $\delta\epsilon_{\mathbf{k}}$ as:

$$\delta\epsilon_{\tilde{\mathbf{k}}_0} \approx \frac{1}{2}\sum_{\mathbf{q}} \frac{\left|\Phi_1(\tilde{\mathbf{k}}_0,\mathbf{q})\right|^2}{w[\tilde{\mathbf{k}}_0,\mathbf{q}]}, \tag{31}$$

for simplicity. Then we consider the numerator in the limit of $\mathbf{q} \to 0$ by Eqs. (30) and (31):

$$\frac{2NS\left|\Phi_1(\tilde{\mathbf{k}}_0,\mathbf{q})\right|^2|_{\mathbf{q}\to 0}}{(H\cos\theta)^2} \approx \frac{9}{16}\frac{k_0^3}{(2\sqrt{2}\cos\theta)^3}, \tag{32}$$

and obtain Eq. (21).

The denominator $w[\tilde{\mathbf{k}}_0,\mathbf{q}]$ is approximated by [2]:

$$|\mathbf{k}/2+\mathbf{q}| = k/2 + q - \frac{1}{4}\frac{kq}{(k/2+q)^2}\phi^2. \tag{33}$$

We get Eq. (22) by using:

$$\begin{aligned} w[\tilde{\mathbf{k}}_0,\mathbf{q}] \approx c\,\big[&k_0 - |\mathbf{k}_0/2+\mathbf{q}| - |\mathbf{k}_0/2-\mathbf{q}| \\ &+\alpha\left(k_0^3 - |\mathbf{k}_0/2+\mathbf{q}|^3 - |\mathbf{k}_0/2-\mathbf{q}|^3\right)\big]. \end{aligned} \tag{34}$$

We now obtain Eq. (23) by using Eqs. (21) and (22).

B ESTIMATION OF ROTON MASS

We obtain k_0 dependence of $m_\perp/m_\parallel$ by differentiating $\delta\epsilon_{\mathbf{k}}$ perpendicular/parallel to the Γ-M line.

We differentiate $\bar{\epsilon_{\mathbf{k}}}$ perpendicular to the line:

$$\begin{aligned} 1/m_\perp^* \approx & \frac{1}{k_0}\frac{\partial \delta\epsilon_{\tilde{\mathbf{k}}_0}}{\partial k_0} \\ = & \frac{1}{2k_0}\sum_{\mathbf{q}}\left[\frac{\partial}{\partial k_0}\left(\frac{1}{w[\tilde{\mathbf{k}}_0,\mathbf{q}]}\right)\left|\Phi_1(\tilde{\mathbf{k}}_0,\mathbf{q})\right|^2\right. \\ & \left. + \left(\frac{1}{w[\tilde{\mathbf{k}}_0,\mathbf{q}]}\right)\frac{\partial\left|\Phi_1(\tilde{\mathbf{k}}_0,\mathbf{q})\right|^2}{\partial k_0}\right], \end{aligned} \tag{35}$$

and parallel to the line:

$$\begin{aligned} 1/m_\parallel^* \approx & \frac{\partial^2(\epsilon_{\tilde{\mathbf{k}}_0}+\delta\epsilon_{\tilde{\mathbf{k}}_0})}{\partial k_0^2} \\ = & d_0 k_0^3 \\ & + \frac{1}{2}\sum_{\mathbf{q}}\left[\frac{\partial}{\partial k_0}\left(\frac{2}{w[\tilde{\mathbf{k}}_0,\mathbf{q}]}\right)\frac{\partial\left|\Phi_1(\tilde{\mathbf{k}}_0,\mathbf{q})\right|^2}{\partial k_0}\right. \\ & + \frac{1}{w[\tilde{\mathbf{k}}_0,\mathbf{q}]}\frac{\partial^2\left|\Phi_1(\tilde{\mathbf{k}}_0,\mathbf{q})\right|^2}{\partial k_0^2} \\ & \left. + \left|\Phi_1(\tilde{\mathbf{k}}_0,\mathbf{q})\right|^2\frac{\partial^2}{\partial k_0^2}\left(\frac{1}{w[\tilde{\mathbf{k}}_0,\mathbf{q}]}\right)\right], \end{aligned} \tag{36}$$

where d_0 denotes a constant and we use:

$$\begin{aligned} \frac{\partial^2\epsilon_{\mathbf{k}_0}}{\partial k_0^2} \approx & \frac{\partial^2}{\partial k_0^2}\left(ck_0+\frac{\alpha k_0^3}{5}\right) \\ \propto & k_0^3. \end{aligned} \tag{37}$$

We obtain an approximation to differentiated $w[\mathbf{k}_0,\mathbf{q}]$ by:

$$\begin{aligned} \frac{\partial}{\partial k_0}\left(\frac{1}{w[\tilde{\mathbf{k}}_0,\mathbf{q}]}\right) = & -\frac{1}{w[\tilde{\mathbf{k}}_0,\mathbf{q}]^2}\frac{\partial w[\tilde{\mathbf{k}}_0,\mathbf{q}]}{\partial k_0}, \\ \frac{\partial^2}{\partial^2 k_0}\left(\frac{1}{w[\tilde{\mathbf{k}}_0,\mathbf{q}]}\right) = & \frac{2}{w[\tilde{\mathbf{k}}_0,\mathbf{q}]^3}\left(\frac{\partial w[\tilde{\mathbf{k}}_0,\mathbf{q}]}{\partial k_0}\right)^2 \\ & - \frac{1}{w[\tilde{\mathbf{k}}_0,\mathbf{q}]^2}\frac{\partial^2 w[\tilde{\mathbf{k}}_0,\mathbf{q}]}{\partial k_0^2}. \end{aligned} \tag{38}$$

and using Eq. (22):

$$\begin{aligned} \frac{\partial w[\tilde{\mathbf{k}}_0,\mathbf{q}]}{\partial k_0} \approx & \frac{2cq^2}{k_0^2}(\phi^2+3\phi_0^2), \\ \frac{\partial^2 w[\tilde{\mathbf{k}}_0,\mathbf{q}]}{\partial k_0^2} \approx & -\frac{4cq^2}{k_0^3}(\phi^2-3\phi_0^2). \end{aligned} \tag{39}$$

We now obtain $m_\perp$ and $m_\parallel$ by using Eqs. (35), (36), (38), (39), and derivatives of matrix elements [see Eq. (21)] with respect to k_0. We now obtain Eqs. (25) and (26).

References

[1] R. Coldea, S. M. Hayden, G. Aeppli, T. G. Perring, C. D. Frost, T. E. Mason, S.-W. Cheong, and Z. Fisk: Phys. Rev. Lett. **86** (2001) 5377.

[2] M. Mourigal, M. E. Zhitomirsky, and A. L. Chernyshev: Phys. Rev. B **82** (2010) 144402.

[3] M. E. Zhitomirsky and A. L. Chernyshev: Phys. Rev. Lett. **82** (1999) 4536.

[4] M. E. Zhitomirsky and A. L. Chernyshev: Rev. Mod. Phys. **85** (2013) 219.

[5] A. Lüscher and A. M. Läuchli: Phys. Rev. B **79** (2009) 195102.

[6] A. L. Chernyshev and M. E. Zhitomirsky: Phys. Rev. B **79** (2009) 144416.

[7] W. Zheng, J. O. Fjærestad, R. R. P. Singh, R. H. McKenzie, and R. Coldea: Phys. Rev. B **74** (2006) 224420.

[8] O. F. Syljuåsen: Phys. Rev. B **78** (2008) 180413.

[9] T. Masuda, S. Kitaoka, S. Takamizawa, N. Metoki, K. Kaneko, K. C. Rule, K. Kiefer, H. Manaka, and H. Nojiri: Phys. Rev. B **81** (2010) 100402.

[10] N. Tsyrulin, T. Pardini, R. R. P. Singh, F. Xiao, P. Link, A. Schneidewind, A. Hiess, C. P. Landee, M. M. Turnbull, and M. Kenzelmann: Phys. Rev. Lett. **102** (2009) 197201.

[11] J. Oh, M. D. Le, J. Jeong, J.-h. Lee, H. Woo, W.-Y. Song, T. G. Perring, W. J. L. Buyers, S.-W. Cheong, and J.-G. Park: Phys. Rev. Lett. **111** (2013) 257202.

[12] T. Ono, K. Matan, Y. Nambu, T. J. Sato, K. Katayama, S. Hirata, and H. Tanaka: J. Phys. Soc. Jpn. **83** (2014) 043701.

[13] W. T. Fuhrman, M. Mourigal, M. E. Zhitomirsky, and A. L. Chernyshev: Phys. Rev. B **85** (2012) 184405.

[14] M. E. Zhitomirsky and T. Nikuni: Phys. Rev. B **57** (1998) 5013.

[15] R. A. Cowley and A. D. B. Woods: Can. J. Phys. **49** (1971) 177.

[16] A. L. Chernyshev and M. E. Zhitomirsky: Phys. Rev. B **79** (2009) 174402.

[17] A. V. Chubukov and O. A. Starykh: Phys. Rev. Lett. **110** (2013) 217210.

[18] D. S. Greywall: Phys. Rev. B **18** (1978) 2127.

[19] P. A. Goddard, J. Singleton, P. Sengupta, R. D. McDonald, T. Lancaster, S. J. Blundell, F. L. Pratt, S. Cox, N. Harrison, J. L. Manson, H. I. Southerland, and J. A. Schlueter: New J. Phys. **10** (2008) 083025.

[20] Y. Kubo and S. Kurihara: J. Phys. Soc. Jpn. **82** (2013) 113601.